Journal of
Nanomedicine & Nanotechnology

Szekeres et al., J Nanomed Nanotechnol 2015, 6:1
DOI: 10.4172/2157-7439.1000252

Research Article Open Access

Hemocompatibility and Biomedical Potential of Poly(Gallic Acid) Coated Iron Oxide Nanoparticles for Theranostic Use

Márta Szekeres[1]*, Erzsébet Illés[1], Christina Janko[2], Katalin Farkas[3], Ildikó Y Tóth[1], Dániel Nesztor[1], István Zupkó[4], Imre Földesi[3], Christoph Alexiou[2] and Etelka Tombácz[1]*

[1]*Department of Physical Chemistry and Materials Science, University of Szeged, Aradi vt 1, 6720 Szeged, Hungary*
[2]*Department of Otorhinolaryngology, Head and Neck Surgery, Section for Experimental Oncology and Nanomedicine (SEON), University Hospital Erlangen, Glückstraße 10a, 91054 Erlangen, Germany*
[3]*Institute of Laboratory Medicine, Faculty of Medicine, University of Szeged, Semmelweis u. 6, 6720 Szeged, Hungary*
[4]*Department of Pharmacodynamics and Biopharmacy, University of Szeged, Eötvös u. 1, 6720 Szeged, Hungary*

Abstract

Polyacid covered core-shell iron oxide nanoparticles were designed for potential use in biomedicine with special attention to theranostics - magnetic resonance imaging (MRI), magnetic hyperthermia and magnetic drug targeting. The magnetite nanoparticles coated with a gallic acid shell polymerized *in situ* on the nanoparticle surface (PGA@MNPs) were tested for hemocompatibility in blood, sedimentation rate, blood smear and blood cell viability experiments and for antioxidant capacity in Jurkat cells in the presence of H_2O_2 as reactive oxygen species. No signs of interaction of the nanoparticles with whole blood cells were found. In addition, the PGA@MNPs reduced significantly the oxidative stress mediated by H_2O_2 supporting earlier findings of MTT tests, namely, the improvement of cell viability in their presence. The *in vitro* tests revealed that PGA@MNPs are not only biocompatible but also bioactive. Preliminary experiments revealed that the nanoparticles are especially efficient MRI and magnetic hyperthermia agents. The r^2 relaxivity was found to be one of the highest among published values (387 $mM^{-1}s^{-1}$) and they possess a relatively significant specific absorption rate (SAR) value of 11 W/g magnetite.

Keywords: Iron oxide nanoparticles; HeLa, Jurkat and blood cells; Hemocompatibility; Antioxidant effect; MRI contrast enhancement; Magnetic hyperthermia

Introduction

A wide variety of core-shell magnetic iron oxide (magnetite) nanoparticles (MNPs) has been designed up to date for the aims of magnetic imaging (magnetic resonance imaging, MRI; magnetic particle imaging, MPI), magnetic hyperthermia and targeted drug delivery [1-10]. The combined use of MNPs in both diagnosis and therapy (called theranostics) exploits the superparamagnetic property of nano-sized magnetite (also called SPION, "superparamagnetic iron oxide nanoparticle") and its specific surface properties that allow easy surface modification by physical or chemical adsorption of different organics. The shell around the core particles ensures colloidal stability and salt tolerance, which are necessary to prevent aggregation in the biological environment. In addition, the coating layer can host biologically active molecules such as drugs and targeting agents.

Using surface-polymerized gallic acid (PGA) as protecting shell of nanoparticles can be highly advantageous in biomedicine, because gallic acid (GA) is not only biocompatible but also bioactive. GA is one of the most important antioxidant components of a healthy diet. The anti-inflammatory, antibiotic, antifungal and anticancer effects of GA are well known as well as its role in preventing cardiovascular diseases and neurodegenerative disorders [11-15]. Many GA-like compounds (phenolic acids) are present in large concentrations in different plants [16]. GA has been used as a model for food polyphenols [17] and the concentration of dietary polyphenols is often expressed in gallic acid equivalents. GA-like compounds are also used in biomedicine as drugs for toxic metal removal due to their capability of chelating heavy metal and transition metal ions [18]. Their application for curing degenerative diseases is promising, because they can cross the blood brain barrier and chelate toxic ions in the brain thus preventing or even inverting the formation of plaques [13,14]. When attached to magnetic nanoparticles, the curing efficiency can be enhanced via magnetic targeting.

We prepared GA-coated magnetite nanoparticles and allowed surface-induced polymerization to proceed during the course of five weeks resulting in PGA-coated MNPs (PGA@MNP). Our hypothesis was that the autogenic polymerization of GA catalyzed by the surface of MNPs should proceed similarly to the known natural process of humic matter formation on the surface of clay minerals, the precursor molecules of which are structurally similar to GA [19]. This way, the synthesis of PGA@MNPs would proceed in an all-natural soft method and the emergence of toxic by-products would be excluded. The PGA@MNPs have indeed been successfully produced and we have published their physico-chemical and colloidal characterization relevant to possible biomedical applications [20-22]. In the present study, we utilized *in vitro* experiments for testing the biodistribution, biocompatibility and antioxidant capacity of the polygallate stabilized SPION product. In addition, we studied the MRI contrasting and hyperthermia efficiency of the coated MNPs.

Materials and Methods

$FeCl_2 \cdot 4H_2O$, $FeCl_3 \cdot 6H_2O$ (Molar, Hungary), gallic acid (GA, Carlo

***Corresponding authors:** Szekeres M, Department of Physical Chemistry and Materials Science, University of Szeged, Aradi vt 1, 6720 Szeged, Hungary, Tel: 36-62544212; E-mail: szekeres@chem.u-szeged.hu

Tombácz E, Department of Physical Chemistry and Materials Science, University of Szeged, Aradi vt 1, 6720 Szeged, Hungary, Tel: 36-62544212; E-mail: tombacz@chem.u-szeged.hu

Received October 13, 2014; **Accepted** December 10, 2014; **Published** January 01, 2015

Citation: Szekeres M, Illés E, Janko C, Farkas K, Tóth IY, et al. (2015) Hemocompatibility and Biomedical Potential of Poly(Gallic Acid) Coated Iron Oxide Nanoparticles for Theranostic Use. J Nanomed Nanotechnol 6: 252. doi: 10.4172/2157-7439.1000252

Erba) and NaCl, NaOH and HCl (Molar, Hungary) to set the ionic strength and pH in the experiments were analytical grade reagents. Ultrapure water (18 MΩ) from a HumanCorp Zeneer water purification system was used in the experiments.

Magnetite (Fe_3O_4) nanoparticles were synthesized by alkaline hydrolysis of iron(II) and iron(III) salts [22]. Briefly, the concentrated iron salt solutions were mixed at the ratio of 1:2 and precipitated by NaOH solution. We washed and acidified the formed MNPs in order to fully disperse them in the aqueous medium, then dialyzed against 1 mM HCl solution and stored in the dark at 4°C.

The PGA@MNPs for the biomedical tests were prepared on the basis of GA adsorption experiments detailed by us earlier [21,22]. The PGA@MNP dispersions were prepared at a concentration of 15 g/L in aqueous medium. The pH of magnetite dispersions was adjusted to ~6.5 and GA was added in concentration of 0.6 mmol GA/g magnetite. The pH was readjusted subsequently for five weeks, during which period GA polymerized at the surface as it is demonstrated in [21,22]. The sample was stored in dark at 4°C. The values of electrokinetic potential (-40 mV), hydrodynamic diameter (~170 nm, as compared to that of naked MNPs of ~100 nm) and critical coagulation concentration (500 mM, while that of naked MNPs of is only 1 mM) revealed the presence of a thick coating layer, which in turn, stabilizes the particles even in the presence of salt at high concentrations. TEM pictures of naked and PGA-coated MNPs are given in Seciton 1 of Supplementary material (Figures S1 and S2) demonstrating also the formation of a thick PGA coating. Particles with not fully polymerized GA shell (GA@MNPs) were also characterized earlier [21,22]. Although they were found to be highly biocompatible (cell viability inhibition < 5%), their low colloidal stability made them inapplicable for biomedical application.

Interaction of PGA@MNPs with HeLa cells

The accumulation of PGA@MNPs at the surface of or inside cancer cells was tested via examining their interaction with HeLa cells in a cell culture within 48 hours using Prussian blue staining. The procedure is described in detail in [22].

Hemocompatibility tests

Hemocompatibility of PGA@MNPs, i.e. their interaction with human blood was studied in erythrocyte sedimentation rate (ESR) experiments utilizing a Sedi-15 automated sedimentation rate measuring device (BD Inc., Franklin Lakes, NJ, USA) and Seditainer 1.8 vacutainer tubes (BD Inc., USA) as given in our previous publication [22]. PGA@MNP samples were mixed at room temperature with citrate-, and EDTA-anticoagulated blood of three healthy donors (Donors #1-#3) to achieve a PGA@MNP concentration of 0.32 mg/mL.

Peripheral blood smear tests of the whole blood (EDTA-anticoagulated) of the donors were carried out by an automated slide preparation system (Sysmex SP4000i) at room temperature using the May-Grünwald Giemsa (MGG, Biolyon, Dardilly, France) staining technique in a CellaVisionTM DM96 automation device (CellaVision AB, Ideon, Science Park, Lund, Sweden) as detailed in [22]. The influence of PGA@MNPs on platelet aggregation was studied at a concentration of 0.32 mg/mL. The acquisition and classification software of the instrument was used to differentiate the normal and abnormal cells (white blood cells (WBC), red blood cells (RBC) and platelets (PLT)).

Blood cell viability measurements

WBC viability factor (WVF), i.e., the fraction of viable WBCs present in the sample was determined by CELL-DYN Sapphire hematology analyser (Abbott Diagnostics, USA). This routine diagnostic method is used to differentiate the necrotic, apoptotic and normal cells in EDTA-anticoagulated blood based on the selective staining of nuclei of damaged or nonviable cells with a cell membrane impermeable fluorescent dye, propidium iodide. After hydrodynamic focusing, WVF was determined by the emitted red fluorescence (at 617 nm) of the dye bound to the nucleic acid of injured or dead cells. The effect of PGA coated nanoparticles on WBC viability was examined at 37°C. PGA@MNP concentration in blood was 0.4 mg/mL. The WVF values were determined 10, 30, 60, 90, 120, 180 and 240 minutes after mixing the MNPs with the blood of Donors #1-#3 at a final concentration of 0.4 mg PGA@MNP/mL. The accuracy of the measured WVFs is above 97% as calculated from 5 parallel runs. The cell count of WBC, RBC and PLT comprising all viable, damaged and dead cells was determined by impedance measurements in the same samples. The impedance measurements were also used for determination of the volumes of thrombocytes and red blood cells.

Determination of antioxidant capacity

The non-adherent human T-cell leukemia cell line Jurkat (DSMZ ACC 282) was used for *in vitro* experiments. The cells were cultured in RPMI medium supplemented with 10% fetal calf serum and 1 % glutamine (all from Thermo Fisher Scientific, Waltham, MA, USA) under standard cell culture conditions in a humidified incubator at 37°C and 5% CO_2. For the experiments, the cells were counted and their viability was determined using MUSE Cell Analyzer (Merck Millipore, Billerica, MA, USA). The antioxidative capacity of free GA and PGA@MNPs was determined according to the following procedure. Intracellular oxidative stress was determined using 2′,7′-Dichlorofluorescein diacetate (DCFH-DA, Sigma-Aldrich, Taufkirchen, Germany). The cells were adjusted to a density of 5×10^5 / mL in PBS (Gibco, Thermo Fisher Scientific, Waltham, MA, USA) and pre-incubated with 20 μM DCFH-DA for 30 minutes at 37°C. Then the cells were washed once with PBS and subsequently incubated in cell culture medium with free GA or PGA@MNPs in the indicated concentrations for 1 h at 37°C without further washing steps. As an oxidizing agent H_2O_2 (Roth, Karlsruhe, Germany) was added to the cells for further 2 h at 37°C. Then the cells were analyzed using a Gallios flow cytometer (Beckman Coulter, Fullerton, CA, USA). Intracellular DCF fluorescence (excitation at 488 nm and emission at 525 nm) was measured by gating of morphologically viable cells. Data analysis was performed with Kaluza software version 2.0 (Beckman Coulter).

MRI studies

The MRI contrast enhancement efficiency of the PGA@MNP was studied by determining the T_1 (longitudinal) and T_2 (transversal) relaxation times and calculating r_1 and r_2 relaxivities as described in our previously published paper [23] by using a clinical MRI instrument GE Excite HDxt (GE Medical Systems, Milwaukee, WI) at magnetic field strength of 1.5 T. The contrast enhancement of coated particles was measured using the standard "birdcage" head coil. The MNP dispersions were prepared at nominal Fe concentrations of 0.009, 0.018, 0.045, 0.09, 0.135, 0.18 and 0.22 mM and the exact iron content of the samples was measured by inductively coupled plasma (ICP) method using an Optima 7000 DV ICP-OES instrument (Perkin-Elmer, Shelton, CT, USA). 4 mL of samples was placed in a plastic box filled with water and put in the centre of the head coil. The r_1 and r_2 relaxivities were determined as the slopes of the $1/T_1$ and $1/T_2$ vs. Fe concentration plots to quantify the contrast enhancement efficiency of

the PGA@MNPs. The quality of fitting was estimated by the coefficient of determination (R-squared).

Hyperthermia experiments

The magnetic hyperthermia efficiency of PGA@MNPs was tested in a magneTherm™ (nanoTherics Ltd., Keele, Staffordshire, UK) instrument. The volume of the MNP dispersion was 4 mL, and the concentration 15 g/L. The measurements were performed at a resonant frequency of 110.7 kHz in a magnetic field of B=25 mT (H=19.9 kA/m, 17 turn coil and 200 nF capacitor). The measurement time in the hyperthermia setup was 15 minutes and the specific absorption rate (SAR, W/g magnetite) values for the initial rate of temperature change were calculated according to the approximating equation (Eq.1):

$$SAR=(c_{p,s}\, m_{water}/m_{PGA@MNP})\,(\Delta T/\Delta t) \quad (1)$$

where $c_{p,s}$ is the specific heat capacity of the medium (water), m_{water} and $m_{PGA@MNP}$ are the masses of the medium and the nanoparticles, respectively, and $\Delta T/\Delta t$ is the initial temperature rate.

Results and Discussion

Interaction of PGA@MNPs with Hela cells

The Prussian blue staining method allowed detecting the distribution of PGA@MNPs in the matrix of a HeLa cancer cell culture. As it is seen in Figure 1, the particles contacted with the cancer cells intimately either by adsorbing at the outer surface or by penetrating into the cytoplasm. The adsorption was observed as the presence of particle agglomerates linked to the cells. In case of penetration, the nuclei remained unstained. Both types of interaction are advantageous for the medical use of the particles. The attachment to the surface and internalization identify the cancer cells in MRI and localize the heat production in hyperthermia. The PGA@MNPs can also be used for targeting specific anticancer drugs, which extends their potential use in the wider field of theranostics. The tendency of cells to internalize negatively charged core-shell nanoparticles, such as GA@MNPs at physiological pH [20], has been reported frequently [24].

Hemocompatibility of PGA@MNPs

Three standard *in vitro* assays [25,26], blood sedimentation (i.e., erythrocyte sedimentation rate, ESR), smear and WBC viability tests were used to assess the hemocompatibility of PGA@MNPs. Blood sedimentation experiments were performed with citrate-anticoagulated blood samples to examine whether the coated magnetic nanoparticles induce RBC aggregation or not. Although the citrate anticoagulant seems to induce thrombocyte aggregation [22], it can be safely used for blood sedimentation rate measurements in accordance with the daily laboratory routine, since it does not influence the sedimentation of RBCs. In addition, the thin and long citrate-anticoagulated test tubes are suited well for visual observations similarly to the EDTA-anticoagulated tubes, but use significantly smaller sample volume. Representative sedimentation results are shown in Figure 2. The height of the settled RBCs is virtually the same both in the absence and the presence of PGA@MNPs, but a brownish colour appeared in the plasma after addition of PGA@MNPs. Similar effect was found for other types of polyacid-coated MNPs as well [22,27]. The recorded ESR values coincide in the absence and presence of coated MNPs (11 and 8 mm/h, respectively) within the formal accuracy of the measurements ±3 mm/h. The same RBC sedimentation feature was observed in EDTA-anticoagulated test tubes as well. The presence of PGA@MNP did not influence the aggregation of RBCs in either of the experiments. The same picture was observed previously when GA-coated MNPs (GA adsorbed but not polymerized) were added to whole blood samples [22], with ESR value of 9 mm/h. This suggests that hemocompatibility is determined by the chemistry of the surface of MNPs but does not depend on the thickness of the coating layer.

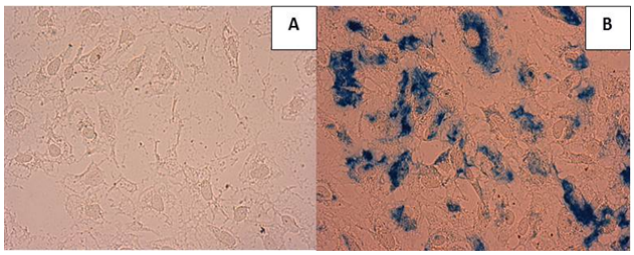

Figure 1: Prussian blue staining of HeLa cell culture. (A) Control and (B) PGA@MNP loading at 7.35 mg/mL concentration.

Figure 2: Blood sedimentation test of native blood sample of Donor #3 (left) and of blood-PGA@MNP mixture at 0.32 mg/mL PGA@MNP concentration (right).

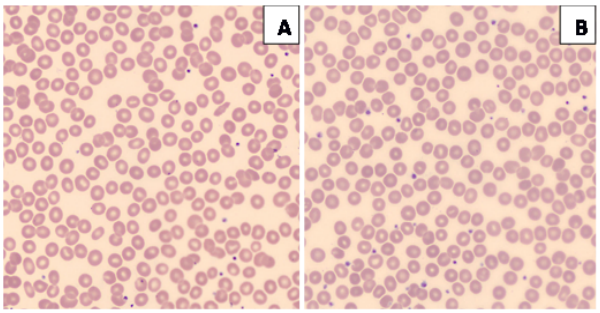

Figure 3: Microscopic pictures of the blood smears prepared from EDTA-anticoagulated blood of Donor #3 (A) without and (B) with PGA@MNPs.

Peripheral blood smear tests were performed to study the influence of MNPs on platelet aggregation. EDTA-anticoagulated blood samples were used to exclude thrombocyte aggregation observed previously in citrate-anticoagulated blood [22]. The morphological analysis of human blood cells showed neither deformation nor decomposition of RBCs in the presence of PGA coated nanoparticles. As it is seen in Figure 3, no aggregation of RBCs was detected revealing excellent hemocompatibility of PGA@MNPs comparable to that of other polyacid- [22,27], polyethylehene oxide (PEG)- [23] and

dehydroascorbic acid (DHA)- [28] coated MNPs. Similar pictures were taken for all the three donor's blood.

The effect of PGA@MNP on viability of white blood cells (WBCs) was tested by measuring the viability factor (WVF) and the results obtained for the blood of Donor #3 are demonstrated in Figure 4. The viable fraction of WBCs of EDTA-coagulated native blood decreased from 0.99 to 0.97 after 240 minutes, which is a spontaneous process in *in vitro* experiments. The oxygen and nutrients concentration of blood decreases with time initiating a gradual cell death right after the sample collection [26]. The PGA coated nanoparticles were dispersed in an aqueous medium and so the effect of the added water on the WBC viability was studied as well. Addition of ultrapure water induced a decrease in WVF from 0.98 to 0.91 within 240 minutes. The dilution caused a stronger decrease in WVF as compared to the undiluted sample probably due to the decrease in the osmotic pressure and an additional decrease in nutrient content [26]. No further change in the time-dependence of WVF was observed upon addition of PGA@MNP revealing the excellent hemocompatibility of the PGA coated nanoparticles. The relatively empty right region of scatter plot of the blood containing PGA@MNPs (inset of Figure 4) shows that only negligible amount of necrotic and apoptotic cells are present in the sample. The same picture was observed for the water-diluted blood sample, indicating that WBC viability was influenced by dilution, but not by the presence of PGA coated nanoparticles. Similar results were obtained for the blood samples of Donors #1 and #2.

Exploiting the multichannel structure of the CELL-DYN Sapphire hematology analyzer, we investigated the change in the cell counts of RBC, WBC and PLT in parallel as a function of time, dilution and PGA@MNP addition. The results are shown in Figure 5. The total amount of the three blood components did not change significantly during the 240 minutes of the experiment, indicating the stability of the blood sample for the time of inspection. Dilution with ultrapure water reduced the cell count values of WBC, RBC and PLT and the decrease coincided well with the degree of dilution (16%) for all three components. Dilution with PGA@MNP dispersion led to the same ~16% decrease in the cell counts evidencing that the presence of the nanoparticles did not affect the stability of the sample.

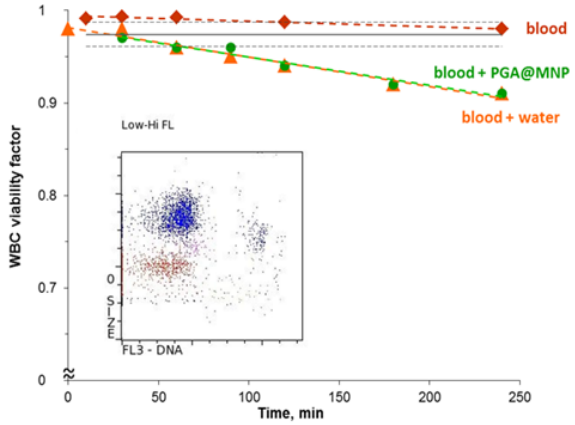

Figure 4: Time-dependent WBC viability in EDTA-anticoagulated blood with and without PGA@MNPs. Inset: Fluorescence scatter plot of blood samples with PGA@MNPs. FL3-DNA is the fluorescence intensity of DNA-bound propidium iodide and SIZE is cell size determined from intensity loss. The blue and red dots indicate different types of WBC.

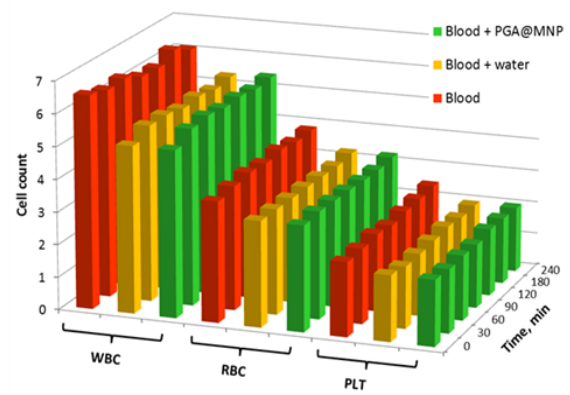

Figure 5: Time-dependent change in the cell count of WBCs (6.5-5×10^6 /L), RBCs (3.7-3.2×10^9 /L) and PLTs (2.4-2×10^4 /L) in the blood sample of Donor #3 without dilution and diluted with water and PGA@MNP dispersion at 37°C.

The mean platelet volume (MPV=8.47 ± 0.2 10^{-15} L) did not change with time in the blood-PGA@MNP mixture, which also supports the results from smear experiments that no thrombocyte aggregation occurred in the presence of PGA coated nanoparticles. However, a slight increase was observed in the mean RB cell volume over time (Δ MCV ~2%, from 87.9 to 90.0 10^{-15} L) indicating that swelling took place during the experiments. This can be explained either by the change in the osmotic conditions after dilution or by thermal instability of RBCs as the temperature-dependence of their swelling property was observed in other human studies as well [29]. The hemocompatibility experiments, altogether, did not show any tendency for PGA@MNPs to interfere negatively with any of the blood components considered in our experiments. This evidence of hemocompatibility makes the particles good candidates for use as MRI or drug targeting agents being injected intravenously.

Antioxidant effect of PGA@MNPs

The effect of free GA or PGA@MNPs on the cellular morphology of Jurkat cells was analyzed in flow cytometry by means of forward scatter (FS) and side scatter (SS) (shown in Figure S3A, Section 2 of Supplementary material), providing information about cellular size and granularity. Cells undergoing cell death change their morphology, reflected by scatter alterations [30], thus viable cells can be clearly separated from dying or dead cells [31]. Morphological analysis showed that treatment of Jurkat cells with low concentrations of H_2O_2 (25 μM and 50 μM) and/or GA solutions only induced minimal amounts of cell death during the observation period of 2 h.

Intracellular oxidative stress was determined using the cell permeable non-fluorescent dye DCFH-DA, which is enzymatically hydrolyzed inside the cells by cellular esterases to non-fluorescent DCFH. In the presence of oxidative stress, DCFH is subsequently oxidized to fluorescent DCF [32]. To be sure that the DCF fluorescence is located inside the cells, only cells of the viable gate were considered for analysis of oxidative stress [33]. After treatment with H_2O_2, an increase in the DCF fluorescence was measured as a function of H_2O_2 and GA dosing. Pre-incubation of the cells with free GA significantly reduced the H_2O_2 mediated DCF fluorescence at all tested GA concentrations (shown in Figure S3B, Section 2 of Supplementary material), showing its antioxidative properties.

Next, the question arises whether PGA@MNPs also exhibit

antioxidative capacity or not. Since we speculated that GA might be less potent when immobilized on nanoparticles, we used only the higher nominal GA concentrations 25 μM and 50 μM added in the form of PGA@MNPs. The morphological analysis showed high biocompatibility of PGA@MNPs during the observation period of 2 h (Figure 6A). After induction of oxidative stress using H_2O_2, a dose dependent increase in DCF fluorescence was observed. Adding free GA at 50 μM, as reference, reduced the fluorescence intensity similarly as in the above set of experiments using free GA as antioxidant. Two different PGA@MNP samples were used for the experiments. The first one contained free GA in the supernatant as a result of the adsorption/polymerization process, i.e., dissolved GA in equilibrium with that on the surface of MNPs. Free GA, on the other hand, was removed from the second sample by washing. The PGA@MNP dispersions both with and without free GA reduced the H_2O_2 mediated oxidative stress as it is seen in Figure 6B. However, their effect was weaker as compared to that of free GA. In addition, PGA@MNPs with free GA in the supernatant showed a stronger antioxidative capacity than in the absence of that.

The observed antioxidative capacity of PGA@MNPs is in harmony with our earlier cell viability experiments performed with GA@MNPs on healthy and cancer cells MRC-5, HeLa and A431 for several types of polyacid-coated MNPs [21]. As compared to the cell inhibition values between 3 and 25% found for citrate, humate, polyacrylate and poly(acrylate-*co*-maleate) coated MNPs, for PGA@MNPs we have found negative values around -5% at the highest concentration.

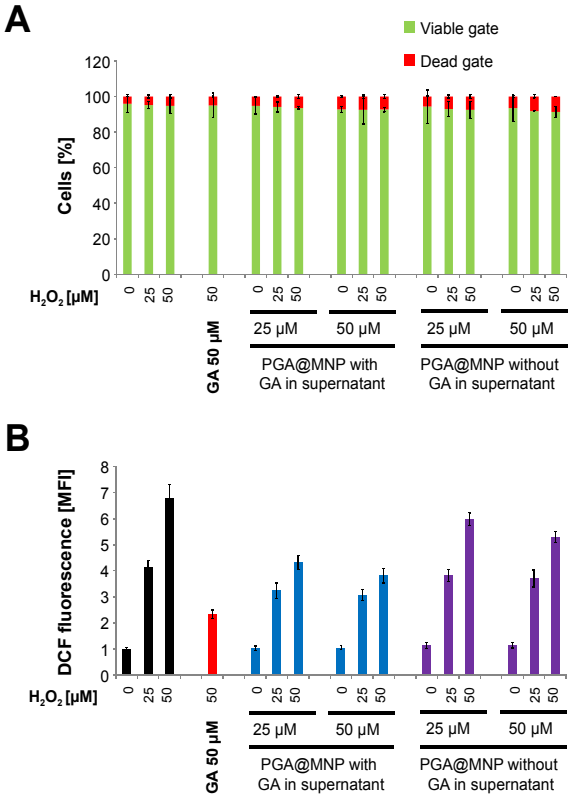

Figure 6: Reduction of H_2O_2mediated oxidative stress by PGA@MNPs. (A) Observed resistance of the cells to morphological changes induced by free GA, PGA@MNPs, or H_2O_2during the observation period of 2 h. (B) The changes in mean fluorescence intensity (MFI) of DCF measured in the population of morphologically viable cells in function of dosing of H_2O_2, free GA and PGA@MNPs.

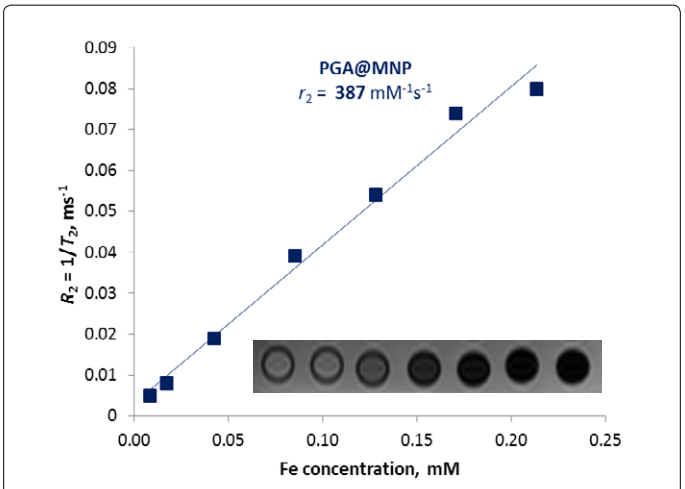

Figure 7: Transverse relaxation rate (R_2=1/T_2) of the PGA@MNP sample as a function of iron concentration and the resulting $r_2$relaxivity value. Inset: T_2-weighted image of samples in phantom water (*TR*=3000 ms, *TE*=40 ms, Fe concentration increases from left to right).

Thus, cell viability has even appeared to be enhanced in the presence of PGA@MNPs in the cell culture. This result becomes fully explicable after their antioxidant effect was experimentally proved in the present studies of oxidative stress reduction.

MRI contrasting properties of PGA@MNPs

The contrast enhancement efficiency of PGA@MNPs was tested in MRI measurements. The longitudinal and transverse relaxivity values (r_1 and r_2, respectively) were calculated by plotting the relaxation rates (R_1=1/T_1 and R_2=1/T_2) against the Fe concentration as described in our previous papers [23,34]. According to our expectations, small r_1 value (1.8 $mM^{-1}s^{-1}$) was obtained for PGA@MNP, which is characteristic for superparamagnetic iron oxide nanoparticles (SPION) in general [23]. However, remarkable T_2 contrast enhancement was recorded for the PGA coated MNPs, shown in Figure 7 as the concentration dependence of the R_2 relaxation rate. The calculated value of transverse relaxivity was extremely high (r_2 ~387 $mM^{-1}s^{-1}$) exceeding the majority of data published for MNPs (50-306 $mM^{-1}s^{-1}$) [28,34-38]. Resovist (r_2 306 $mM^{-1}s^{-1}$) [34], in addition, is generally used as reference superparamagnetic iron oxide MRI contrast agent despite its FDA approval has not yet been completed [22]. The high transverse relaxivity of PGA@MNP is probably due the strong hydration of the highly negatively charged PGA shell near the magnetite core. The enhanced relaxation of large amount of protons near the MNP surface leads to the decrease in signal intensity and increase in the negative contrast [23]. The r_2 relaxivity of PGA@MNPs ~387 $mM^{-1}s^{-1}$ is somewhat lower than that of naked MNPs (measured at pH ~4 as 429.5 ± 9.5 $mM^{-1}s^{-1}$ [34]). The naked MNPs can be stabilized only at low pH, where they hold positive charges due to the accumulation of protons directly on the MNP surface causing the large r_2 relaxivity. In the same time, PGA-coated MNPs are negatively charged (stable in wide range of pH [20], necessary for biocompatibility) and they accumulate water dipoles somewhat farther from the MNP surface, where the effect of the local magnetic field on proton relaxation is weaker.

Magnetic hyperthermia efficiency of PGA@MNPs

The heating effect of two different PGA coated samples was tested and compared to the result obtained for naked MNPs (Figure 8A). The

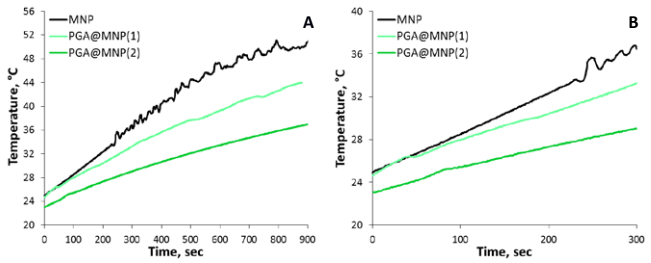

Figure 8: (A) Increase in the temperature of aqueous dispersions of naked and PGA-coated MNPs at particle concentration of 15 mg/mL measured in alternating magnetic field during 15 minutes. (B) The initial part of temperature increase.

gallic acid modified magnetite samples PGA@MNP (1) and PGA@MNP (2) are two different lots produced by the same protocol detailed in the Materials and methods. The frequency and the field strengths (amplitude) of the alternate magnetic field were selected to be appropriate for medical application. The SAR of the MNP and PGA@MNP samples were calculated from the slopes of the heating rate curves below the clear kinks in the PGA@MNP heating rate curves at 70-80 seconds [39] as seen in Figure 8B. The obtained SAR values of all the dispersions were nearly identical, around 11 W/g magnetite. This value is fully consistent with others found in the literature, albeit the choice of the parameters of the magnetic field and the magnetization and particle size of the particles among its other relevant properties have tremendous effect on the SAR values [40-44]. The observed heating efficiency of our samples should be sufficient to rise temperature ~5°C above body temperature necessary to induce apoptosis and necrosis of cells in the case when the same particle concentration can be achieved by accumulating them in specific target locations during administration.

The finding that PGA coating did not alter the SAR of the MNPs is in agreement with the fact that the hyperthermic effect of the nanoparticles with ~8 nm diameter is primarily via Neél relaxation [43], i.e., to the alteration of the direction of a single magnetic dipoles but not the particle as a whole. The coating shell could be expected to affect the heating rate in case of the Brownian type of relaxation or relaxation caused by the obvious magnetic hysteresis of larger magnetic particles.

Conclusions

We have performed *in vitro* biomedical testing of magnetite nanoparticles coated with gallic acid shell polymerized *in situ* at the surface of the particles in a soft and reagent-free process, similar to that of formation of humic matter in nature. The high chemical and colloidal stability of the particles (PGA@MNPs) were studied and discussed thoroughly in our previous publications [20-22], and the paper on the mechanism of surface polymerization of GA on MNPs is published in parallel [45]. The ease and low cost of preparation combined with the exceptional durability and stability of these particles make them superior candidates for biomedical applications.

A series of *in vitro* blood compatibility experiments (ESR, blood smears, viability tests of different particulate components of blood WBC, RBC and PLT) revealed that PGA@MNPs do not interact with whole blood, which make them promising candidates for designing intravenous injection formulations as MRI contrast or drug targeting agents. The significant antioxidant capability of the PGA coating measured in ROS tests may be beneficial in the future *in vivo* applications.

Measurements of r_2 relaxivities for MRI and SAR values for hyperthermia applications proved the reliability of the use of PGA@MNPs as theranostic agents in biomedicine.

Acknowledgement

This work was supported, in part, by the Hungarian Scientific Research Found OTKA (NK84014) and by the Bavarian State Ministry of the Environment and Consumer Protection.

References

1. Chatterjee K, Sarkar S, Rao KJ, Paria S (2014) Core/shell nanoparticles in biomedical applications. Adv Colloid Interface Sci 209: 8-39.
2. Ladja R, Bitar A, Eissa MM, Fessi H, Mugnier Y, et al. (2013) Polymer encapsulation of inorganic nanoparticles for biomedical applications. Int J Pharm 458: 230-241.
3. Figuerola A, Di Corato R, Manna L, Pellegrino T (2010) From iron oxide nanoparticles towards advanced iron-based inorganic materials designed for biomedical applications. Pharmacol Res 62: 126-143.
4. Mahmoudi M, Sant S, Wang B, Laurent S, Sen T (2011) Superparamagnetic iron oxide nanoparticles (SPIONs): Development, surface modification and applications in chemotherapy. Adv Drug Delivery Rev 63: 24-46.
5. Kumar CSSR, Mohammad F (2011) Magnetic nanomaterials for hyperthermia-based therapy and controlled drug delivery. Adv Drug Delivery Rev 63: 789-808.
6. Gupta AK, Gupta M (2005) Synthesis and surface engineering of iron oxide nanoparticles for biomedical applications. Biomaterials 26: 3995-4021.
7. Tietze R, Lyer S, Struffert T, Endgelhorn T, Schwarz M, et al. (2013) Efficient drug-deliviery using magnetic nanoparticles-biodistribution and therapeutic effects in tumour bearing rabbits. Nanomedicine 9: 961-971.
8. Lyer S, Tietze R, Jurgons R, Struffert T, Engelhorn T, et al. (2010) Visualisation of tumour regression after local chemotherapy with magnetic nanoparticles-a pilot study. Anticancer Res 30: 1553-1557.
9. Tietze R, Jurgons R, Lyer S, Schreiber E, Wiekhorst F, et al. (2009) Quantification of drug-loaded magnetic nanoparticles in rabbit liver and tumour after in vivo administration. J Magn Magn Mater 321: 1465-1468.
10. Seliger C, Jurgons R, Wiekhorst F, Eberbeck D, Trahms L, et al. (2007) In vitro investigation of the behavior of magnetic particles by a circulating artery model. J Magn Magn Mater 311: 358-362.
11. Vijayalakshmi G, Adinarayana M, Rao PJ (2010) Kinetics and mechanisms of oxidation of some antioxidants with photochemically generated tert-butoxyl radicals. Indian J Biochem Biophys 47: 292-297.
12. Choe E, Min D B (2009) Mechanisms of Antioxidants in the Oxidation of Foods. Compr Rev Food Sci F 8: 345-358.
13. Mansouri MT, Farbood Y, Sameri MJ, Sarkaki A, Naghizadeh B, et al. (2013) Neuroprotective effects of oral gallic acid against oxidative stress induced by 6-hydroxydopamine in rats. Food Chem 138: 1028-1033.
14. Liu Y, Pukala TL, Musgrave IF, Williams DM, Dehle FC, et al. (2013) Gallic acid is the major component of grape seed extract that inhibits amyloid fibril formation. Bioorg Med Chem Lett 23: 6336-6340.
15. Fiuza SM, Gome C, Teixeira LJ, Girão da Cruz MT, Cordeiro MNDS, et al. (2004) Phenolic acid derivatives with potential anticancer properties -- a structure-activity relationship study. Part 1: Methyl, propyl and octyl esters of caffeic and gallic acids. Bioorg Medicinal Chem 12: 3581-3589.
16. Yilmaz Y, Toledo RT (2004) Major flavonoids in grape seeds and skins: antioxidant capacity of catechin, epicatechin, and gallic acid. J Agric Food Chem 52: 255-260.
17. Chvátalová K, Slaninová I, Brezinová L, Slanina J (2008) Influence of dietary phenolic acids on redox status of iron: Ferrous iron autoxidation and ferric iron reduction. Food Chemistry 106: 650-660.
18. Domingo JL, Ortega A, Llobet JM, Corbella J (1990) Effectiveness of chelation therapy with time after acute uranium intoxication. Fundam Appl Toxicol 14: 88-95.

19. Drosos M, Jerzykiewicz M, Louloudi M, Deligiannakis Y (2011) Progress towards synthetic modelling of humic acid: Peering into the physicochemical polymerization mechanism. Colloids Surf A 389: 254-265.

20. Tombácz E, Tóth IY, Nesztor D, Illés E, Hajdú A, et al. (2013) Adsorption of organic acids on magnetite nanoparticles, pH-dependent colloidal stability and salt tolerance. Colloids Surf A 435: 91-96.

21. Tombácz E, Szekeres M, Hajdú A, Tóth IY, Bauer RA, et al. (2014) Colloidal stability of carboxylated iron oxide nanomagnets for biomedical use. Period Polytech Chem 58: 3-10.

22. Szekeres M, Tóth IY, Illés E, Hajdú A, Zupkó I, et al. (2013) Chemical and colloidal stability of carboxylated core-shell magnetite nanoparticles designed for biomedical applications. Int J Mol Sci 14: 14550-14574.

23. Illés E, Szekeres M, Kupcsik E, Tóth I Y, Farkas K, et al. (2014) PEGylation of surfacted magnetite core-shell nanoparticles for biomedical application. Colloids Surf A 460: 429-440.

24. Verma A, Stellacci F (2010) Effect of surface properties on nanoparticle-cell interactions. Small 6: 12-21.

25. Szebeni J (2012) Hemocompatibility testing for nanomedicines and biologicals: predictive assays for complement mediated infusion reactions. Eur J Nanomed 4(1): 33-53.

26. Guder WG, Narayanan S, Wisser H, Zawta B (1996) Samples: From the patient to the laboratory, The impact of preanalitical variables on the quality of laboratory results, GIT Verlag GMBH Darmstadt, Germany.

27. Tóth IY, Illés E, Bauer RA, Nesztor D, Szekeres M, et al. (2012) Designed polyelectrolyte shell on magnetite nanocore for dilution-resistant biocompatible magnetic fluids. Langmuir 28: 16638-16646.

28. Gupta H, Paul P, Kumar N, Baxi S, Das DP (2014) One pot synthesis of water-dispersible dehydroascorbic acid coated Fe_3O_4 nanoparticles under atmospheric air: blood cell compatibility and enhanced magnetic resonance imaging. J Colloid Interface Sci 430: 221-228.

29. Freise KJ, Schmidt RL, Gingerich EL, Veng-Pedersen P, Widness JA (2009) The effect of anticoagulant, storage temperature and dilution on cord blood hematology parameters over time. Int J Lab Hematol 31: 496-504.

30. Elstein KH, Zucker RM (1994) Comparison of cellular and nuclear flow cytometric techniques for discriminating apoptotic subpopulations. Exp Cell Res 211: 322-331.

31. Janko C, Munoz L, Chaurio R, Maueröder C, Berens C, et al. (2013) Navigation to the graveyard-induction of various pathways of necrosis and their classification by flow cytometry. Methods Mol Biol 1004: 3-15.

32. Wang H, Joseph JA (1999) Quantifying cellular oxidative stress by dichlorofluorescein assay using microplate reader. Free Radic Biol Med 27: 612-616.

33. Cossarizza A, Ferraresi R, Troiano L, Roat E, Gibellini L, et al. (2009) Simultaneous analysis of reactive oxygen species and reduced glutathione content in living cells by polychromatic flow cytometry. Nat Protoc 4: 1790-1797.

34. Jedlovszky-Hajdú A, Tombácz E, Bányai I, Babos M, Palkó A (2012) Carboxylated magnetic nanoparticles as MRI contrast agents: relaxation measurements at different field strengths. J Magn Magn Mater 324: 3173-3180.

35. Arsalani N, Fattahi H, Nazarpoor M (2010) Synthesis and characterization of PVP functionalized superparamagnetic Fe_3O_4 nanoparticles as an MRI contrast agent. Express Polym Lett 4: 329-338.

36. Tromsdorf UI, Bruns OT, Salmen SC, Beisiegel U, Weller H (2009) A highly effective, nontoxic T_1 MR contrast agent based on ultrasmall PEGylated iron oxide nanoparticles. Nano Lett 9: 4434-4440.

37. Huang J, Zhong X, Wang L, Yang L, Mao H (2012) Improving the magnetic resonance imaging contrast and detection methods with engineered magnetic nanoparticles. Theranostics 2: 86-102.

38. Shao H, Min C, Issadore D, Liong M, Yoon TJ, et al. (2012) Magnetic Nanoparticles and microNMR for Diagnostic Applications. Theranostics 2: 55-65.

39. Dutz S, Hergt R (2014) Magnetic particle hyperthermia-a promising tumour therapy? Nanotechnology 25: 452001.

40. Cervadoro A, Giverso C, Pande R, Sarangi S, Preziosi L, et al. (2013) Design maps for the hyperthermic treatment of tumors with superparamagnetic nanoparticles. PLoS One 8: e57332.

41. Cheraghipour E, Javadpour S, Mehdizadeh AR (2012) Citrate capped superparamagnetic iron oxide nanoparticles used for hyperthermia therapy. J Biomed Sci Eng 5: 715-719.

42. Motoyama J, Hakata T, Kato R, Yamashita N, Morino T, et al. (2008) Size dependent heat generation of magnetite nanoparticles under AC magnetic field for cancer therapy. Biomagn Res Technol 6: 4.

43. Bullivant JP, Zhao S, Willenberg BJ, Kozissnik B, Batich CD, et al. (2013) Materials characterization of Feraheme/Ferumoxytol and preliminary evaluation of its potential for magnetic fluid hyperthermia. Int J Mol Sci 14: 17501-17510.

44. Grüttner C, Müller K, Teller J, Westphal F (2013) Synthesis and functionalisation of magnetic nanoparticles for hyperthermia applications. Int J Hyperthermia 29: 777-789.

45. Tóth IY, Szekeres M, Turcu R, Sáringer Sz, Illés E, et al. (2014) Mechanism of in-situ surface polymerization of gallic acid in an environmental-inspired preparation of carboxylated core-shell magnetite nanoparticles. Langmuir 30: 15451-15461.